

Micromagnetic simulation of μMAG standard problem No. 3: Evaluating the standard dipole-dipole interaction

A. K. F. Silva, D. C. Carvalho, H. S. Assis, and P. Z. Coura

Citation: Chin. Phys. B, 2026, 35 (**1**): 017501. DOI: 10.1088/1674-1056/ae1727
http://cpb.iphy.ac.cn; http://iopscience.iop.org/cpb

What follows is a list of articles you may be interested in

Coupling of magnon modes in nanodisk with spin texture

Zijie Zhou(周子杰), Junning Zhao(赵俊宁), Xinhui Ma(马心慧), Rong Wang(王熔), and Fusheng Ma(马付胜)
Chin. Phys. B, 2025, 34 (**10**): 107506. DOI: 10.1088/1674-1056/ade426

Stability and characteristic modes of skyrmions in magnetic nanotubes

Tijjani Abdulrazak, Qizhi Cai(蔡淇智), and Guangwei Deng(邓光伟)
Chin. Phys. B, 2025, 34 (**10**): 107512. DOI: 10.1088/1674-1056/ade071

Direct observation of ultrafast magnetization dynamics in Co/Ni bit patterned media by time-resolved scanning Kerr microscopy

Wei Zhang(张伟), Wei He(何为), Qin-Li Lv(吕琴丽), Jian-Wang Cai(蔡建旺), Xiang-Qun Zhang(张向群), and Zhao-Hua Cheng(成昭华)
Chin. Phys. B, 2025, 34 (**4**): 047501. DOI: 10.1088/1674-1056/adb67e

Mapping the antiparallel aligned domain rotation by microwave excitation

Jing Zhang(张景), Yuanzhi Cui(崔远志), Xiaoyu Wang(王晓雨), Chuang Wang(王创), Mengchen Liu(刘梦晨), Jie Xu(徐洁), Kai Li(李凯), Yunhe Zhao(赵芸鹤), Zhenyan Lu(陆振烟), Lining Pan(潘丽宁), Chendong Jin(金晨东), Qingfang Liu(刘青芳), Jianbo Wang(王建波), and Derang Cao(曹德让)
Chin. Phys. B, 2024, 33 (**9**): 097506. DOI: 10.1088/1674-1056/ad5536

Shape-influenced non-reciprocal transport of magnetic skyrmions in nanoscale channel

Jie-Yao Chen(陈杰尧), Jia Luo(罗佳), Geng-Xin Hu(胡更新), Jun-Lin Wang(王君林), Guan-Qi Li(李冠祺), Zhen-Dong Chen(陈振东), Xian-Yang Lu(陆显扬), Guo-Ping Zhao(赵国平), Yuan Liu(刘远), Jing Wu(吴竞), and Yong-Bing Xu(徐永兵)
Chin. Phys. B, 2024, 33 (**7**): 077505. DOI: 10.1088/1674-1056/ad34c7

COMPUTATIONAL PROGRAMS FOR PHYSICS

Micromagnetic simulation of μMAG standard problem No. 3: Evaluating the standard dipole–dipole interaction

A. K. F. Silva[†], D. C. Carvalho, H. S. Assis, and P. Z. Coura

Departamento de Física, Laboratório de Simulação Computacional, Universidade Federal de Juiz de Fora, Juiz de Fora, 36036-330 Minas Gerais, Brazil

(Received 5 August 2025; revised manuscript received 16 October 2025; accepted manuscript online 24 October 2025)

Cubic-shaped magnetic particles subjected to a dimensionless uniaxial anisotropy ($Q = 0.1$) aligned with one of the crystallographic axes provide an ideal system for investigating magnetic equilibrium states. In this system, three fundamental magnetization configurations are identified: (i) the flower state, (ii) the twisted flower state, and (iii) the vortex state. This problem corresponds to standard problem No. 3 proposed by the NIST Micromagnetics Modeling Group, widely adopted as a benchmark for validating computational micromagnetics methods. In this work, we approach the problem using a computational method based on direct dipolar interactions, in contrast to conventional techniques that typically compute the demagnetizing field via finite difference-based fast Fourier transform (FFT) methods, tensor grid approaches, or finite element formulations. Our results are compared with established literature data, focusing on the dimensionless parameter $\lambda = L/l_{ex}$, where L is the cube edge length and l_{ex} is the exchange length of the material. To analyze equilibrium state transitions, we systematically varied the size L as a function of the simulation cell number N and intercellular spacing a, determining the critical λ value associated with configuration changes. Our simulations reveal that the transition between the twisted flower and vortex states occurs at $\lambda \approx 8.45$, consistent with values reported in the literature, validating our code (Grupo de Física da Matéria Condensada - UFJF), and shows that this standard problem can be resolved using only interaction dipolar of a direct way without the need for sophisticated additional calculations.

Keywords: micromagnetic simulation, standard problem No. 3, dipolar interaction

PACS: 75.78.–n, 75.78.Cd, 75.40.Mg, 75.10.Hk

DOI: 10.1088/1674-1056/ae1727 **CSTR:** 32038.14.CPB.ae1727

1. Introduction

In ferromagnetic materials like nickel, cobalt, iron, and their alloys below the Curie temperature, the magnetic moments spontaneously align in the same direction. However, different regions in the material can have magnetic moments oriented in distinct directions. The boundary separating regions with different magnetic moment vectors is called domain walls, but if the size of the system is sufficiently small, the magnetic moment vector configuration is unique and can be homogeneous or not. To study processes in magnetic small systems, Schabes *et al.*[1] proposed a numerical investigation of the magnetization process in ferromagnetic cubes (see Fig. 1) via a cubic discretization procedure of the micromagnetic energy functional.

In the calculations of the theoretical model, the following four types of interactions can be taken into account: the external field energy (E_h), an exchange energy (E_{ex}), a magnetostatic energy (E_m) obtained by calculating the demagnetizing field,[2–7] and an uniaxial magnetic anisotropy energy (E_u) (z-axis). Thus, the total energy can be written as

$$E_{total} = E_h + E_{ex} + E_m + E_u. \tag{1}$$

The use of these interactions leads to the definition of the two intrinsic length scales as

$$l_u = \left(\frac{A}{K_u}\right)^{1/2}, \qquad l_{ex} = \left(\frac{A}{K_m}\right)^{1/2}, \tag{2}$$

where A is the exchange stiffness constant, the term $K_m = (1/2)\mu_0 M_s^2$ represents the magnetostatic energy density, M_s is called the saturation magnetization, μ_0 is the vacuum magnetic permeability, and K_u is the uniaxial anisotropy constant. The parameter l_u is the magnetocrystalline exchange length, which scales with the domain wall thickness, while l_{ex} is commonly known as the exchange length. The equilibrium magnetic states are determined by the relative magnitudes of these characteristic lengths (l_u, l_{ex}) compared to the edge length L of the ferromagnetic cube. It is useful to define a dimensionless relative anisotropy

$$Q = \frac{K_u}{K_m}, \tag{3}$$

and a dimensionless length

$$\lambda = \frac{L}{l_{ex}}. \tag{4}$$

The transition between equilibrium configurations can be determined by calculating either the magnetization profile

[†]Corresponding author. E-mail: antonio.kaeliton@estudante.ufjf.br

© 2026 Chinese Physical Society and IOP Publishing Ltd. All rights, including for text and data mining, AI training, and similar technologies, are reserved.

along the z-axis or the energy as a function of the dimensionless length λ. If $Q \ll 1$, the system is very soft; if $0.1 < Q < 1$, it is soft; and if $Q > 1$ it is a hard magnetic material. In 1998, Rave *et al.*[8] published a paper entitled *Magnetic states of small cubic particles with uniaxial anisotropy*, where the magnetic equilibrium states were studied for various values of Q and λ using a micromagnetic formalism. Various equilibrium states such as vortex, twisted vortex, double vortex, and flower were observed.

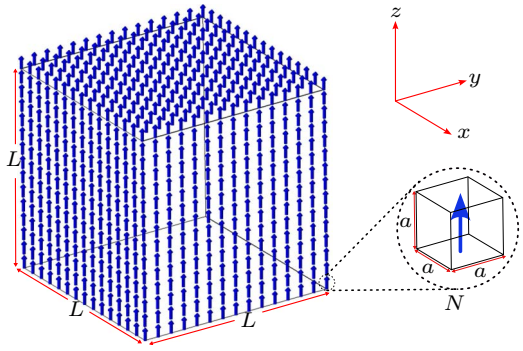


Fig. 1. Illustration of a cubic micromagnetic system composed of N^3 cells prior to relaxation to equilibrium. Each cell has a length a and contains a local resultant magnetic moment.

Due to the possibility of finding well-defined magnetic states of small cubic particles with uniaxial anisotropy calculated by means of the micromagnetic formalism, Hertel *et al.*[9] defined the study of these systems as a problem to be used as a test for micromagnetic simulation of magnetic materials (micromagnetic modeling activity group-μMAG[10]). They focused their study on systems with $Q = 0.1$ and studied the magnetization in the uniaxial direction and energy to determine the changes in the equilibrium states that can occur, such as flower, twisted flower, and vortex (shown in Figs. 2–4, respectively). They found that at $\lambda \approx 8.56$, the vortex state becomes energetically more favorable than the twisted flower state. This problem was called standard problem No. 3, and we applied it to test and validate a program developed by our group using dipolar interaction instead of calculating the demagnetizing field.

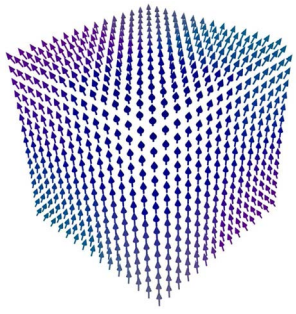


Fig. 2. Magnetization configuration corresponding to the flower state, characterized by a nearly uniform alignment of magnetic moments with slight curling at the edges due to boundary effects.

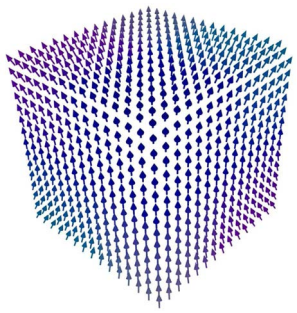


Fig. 3. Magnetization configuration of the twisted flower state, exhibiting a central uniform core with increasing in-plane twisting of magnetic moments towards the cube boundaries.

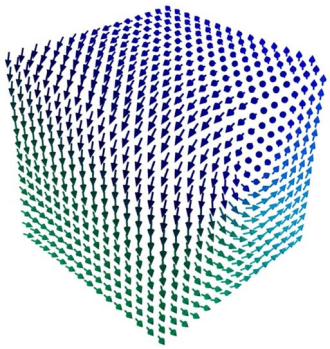


Fig. 4. Magnetization configuration of the vortex state, where magnetic moments circulate around a central core, minimizing magnetostatic energy through flux closure.

2. Methodology

The concept of micromagnetism was initially established by Brown in 1958 with the publication of his book[11] and later with his contributions in published works involving applications of computational methods.[12] It is a continuous theory of magnetic materials that allows the calculation of spin configurations of materials with different shapes.[13]

Magnetic systems are made up of many magnetic moments distributed throughout their structure, with a length scale ranging from tens of nanometers to hundreds of micrometers.[14–16] To measure interactions on this scale, we use micromagnetic simulation, which consists of treating the system through a semiclassical approximation, since approaching these systems through quantum theory becomes highly complex. Then the magnetic moment is represented by a classical vector field

$$\boldsymbol{M}_i = M_{\mathrm{s}} \hat{\boldsymbol{\mu}}_i, \tag{5}$$

with $|\hat{\boldsymbol{\mu}}_i| = 1$, where M_{s} is the saturation magnetization defined in each work cell of the magnetic system. The work cells are obtained by dividing the space into small cuboids with an edge length a (lattice parameter). This way, the Hamiltonian of the system with $NC = N^3$ work cells (N is the number of work cells in each direction) considering only exchange, magnetostatic, and anisotropy energy is given by

$$\mathcal{H} = -\frac{J^{\mathrm{cel}}}{2} \sum_{\langle i,j \rangle}^{NC} \hat{\boldsymbol{\mu}}_i \cdot \hat{\boldsymbol{\mu}}_j$$

$$-\frac{D^{\rm cel}}{2}\sum_{i=1}^{NC}\sum_{\substack{j=1\\ j\neq i}}^{NC}\left[\frac{-\hat{\boldsymbol{\mu}}_i\cdot\hat{\boldsymbol{\mu}}_j+3(\hat{\boldsymbol{\mu}}_i\cdot\hat{\boldsymbol{r}}_{ij})(\hat{\boldsymbol{\mu}}_j\cdot\hat{\boldsymbol{r}}_{ij})}{(r_{ij}/a)^3}\right]$$
$$-K^{\rm cel}\sum_{i=1}^{NC}(\hat{\boldsymbol{\mu}}_i\cdot\hat{\boldsymbol{z}})^2. \tag{6}$$

The first term corresponds to the exchange interaction, where the summation is taken over the nearest magnetic moment pairs $\langle i,j\rangle$. The second term represents the dipole energy or magnetostatic energy calculated using the standard method for a system of magnetic moments distributed in a discrete lattice. The third term is the uniaxial magnetic anisotropy energy. The parameter $J^{\rm cel}=2Aa$ is the micromagnetic exchange coupling constant, $D^{\rm cel}=\mu_0M_{\rm s}^2a^3/4\pi$ is the micromagnetic dipole-dipole coupling constant, and $K^{\rm cel}=K_{\rm u}a^3$ is the uniaxial anisotropy constant. Since $l_{\rm ex}$ is the smallest characteristic length of the system, we must impose the condition

$$a=\xi l_{\rm ex}, \tag{7}$$

with $0<\xi<1$. Thus, $L=Na=N\xi l_{\rm ex}$ and the dimensionless length can be rewritten as

$$\lambda=\frac{L}{l_{\rm ex}}=N\xi. \tag{8}$$

Therefore, the value of λ is determined as a function of the system size N and the proportionality constant ξ, which varies in the interval $0<\xi<1$. For each value of λ, there is a specific corresponding value of ξ, which is the parameter directly adjusted in the simulations. With these definitions, the micromagnetic energy can be expressed in reduced units (R.U) by dividing the total energy by $\mu_0M_{\rm s}^2a^3$ and consequently the constants $J^{\rm cel}$, $D^{\rm cel}$ and $K^{\rm cel}$ can be rewritten in reduced units as follows:

$$J^{\rm cel^*}=\frac{l_{\rm ex}^2}{a^2}=\frac{1}{\xi^2}, \tag{9}$$
$$D^{\rm cel^*}=\frac{1}{4\pi}, \tag{10}$$
$$K^{\rm cel^*}=\frac{Q}{2}. \tag{11}$$

Furthermore, defining the distance between sites in reduced units as $r_{ij}^*=r_{ij}/a$, the Hamiltonian $\mathcal{H}^*$ in reduced units (as a function of Q and ξ), can be written as

$$\mathcal{H}^*=-\frac{J^{\rm cel^*}}{2}\sum_{\langle i,j\rangle}^{NC}\hat{\boldsymbol{\mu}}_i\cdot\hat{\boldsymbol{\mu}}_j$$
$$-\frac{D^{\rm cel^*}}{2}\sum_{i=1}^{NC}\sum_{\substack{j=1\\ j\neq i}}^{NC}\left[\frac{-\hat{\boldsymbol{\mu}}_i\cdot\hat{\boldsymbol{\mu}}_j+3(\hat{\boldsymbol{\mu}}_i\cdot\hat{\boldsymbol{r}}_{ij})(\hat{\boldsymbol{\mu}}_j\cdot\hat{\boldsymbol{r}}_{ij})}{(r_{ij}^*)^3}\right]$$
$$-K^{\rm cel^*}\sum_{i=1}^{NC}(\hat{\boldsymbol{\mu}}_i\cdot\hat{\boldsymbol{z}})^2. \tag{12}$$

However, the goal of this work is to compare the system energy for different values of ξ. According to the relation (7), the edge length a will also change. Since the definition of the exchange energy is formulated without considering the constant term $6Aa$ that arises during the transition from the continuous to the discrete case used in micromagnetism, we include this term to enable a proper comparison of the energy for different values of ξ. This term can be expressed in reduced units by dividing it by $\mu_0M_{\rm s}^2a^3$, resulting in $3N^3/\xi^2$. Thus, we can rewrite the Hamiltonian as $\mathcal{H}^*=\mathcal{H}^*+3N^3/\xi^2$. In this way, the study can be conducted independently of the parameters that characterize the magnetic system. The magnetization dynamics are studied using the Landau–Lifshitz–Gilbert (LLG) equation, which is used to find the equilibrium states[17] and is given by

$$\frac{{\rm d}\hat{\boldsymbol{\mu}}_i}{{\rm d}t^*}=-\frac{1}{1+\alpha^2}\left[\hat{\boldsymbol{\mu}}_i\times\boldsymbol{B}_i^{\rm ef*}+\alpha\hat{\boldsymbol{\mu}}_i\times\left(\hat{\boldsymbol{\mu}}_i\times\boldsymbol{B}_i^{\rm ef*}\right)\right], \tag{13}$$

where $\alpha=0.1$[18,19] is a dimensionless empirical damping parameter, known as the Gilbert damping constant, and $\boldsymbol{B}^{\rm ef*}=-{\rm d}\mathcal{H}^*/{\rm d}\hat{\boldsymbol{\mu}}_i$ is the effective field in reduced units. The choice of integrator depends on the system's definition and what is being measured. In this work, we are interested in minimizing the energy to identify these states. The key point here, therefore, is the energy difference between these states; that is, the error obtained from integrating the equations must be much smaller than this energy difference between the observed states. We have chosen the Adams–Bashforth integrator because it provides stability and precision aligned with the objectives of this work. For better visualization, Fig. 5 shows a comparison between the fourth-order Runge–Kutta method (considered one of the best methods) and the method used in this work. As can be observed, the energy difference between the methods is very small (on the order of decimal places, which is much smaller than the energy difference between the lowest energy states). The only difference lies in the moment when the state change occurs, but this is not important for this work. Thus, we opted to use the Adams–Bashforth method because it is much faster.[20,21]

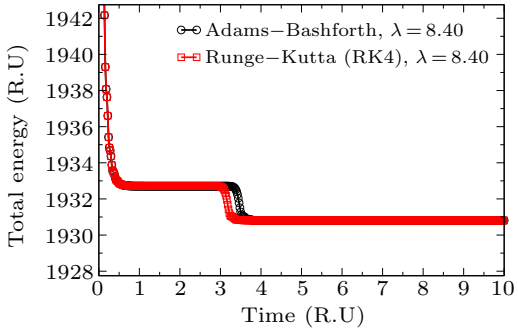


Fig. 5. Total energy as a function of time for $N=15$ and $\lambda=8.40$, using the fourth-order Runge–Kutta and Adams–Bashforth methods. The energy exhibits a small variation over time, confirming the stability and consistency of the method in the micromagnetic simulation. Both time and energy are expressed in reduced units.

The dimensionless time step used was $dt^* = 2 \times 10^{-15}$, and the relation between the real time dt and dt^* is given by $dt^* = \gamma\mu_0 M_s\, dt$, where γ is the electron gyromagnetic ratio.

3. Results and discussion

We vary the number of work cells in the range $9 \leq N \leq 21$ with $Q = 0.1$, using odd values of N to maintain the symmetry of the system relative to the center. In addition, we vary ξ to find the minimum energy states: flower state, twisted flower, or vortex state. Using Eq. (8), we obtained values of λ that are in close agreement with those reported in Refs. [8,9,22–26].

3.1. Flower state

Starting from the initial configuration shown in Fig. 6(a), the system undergoes energy minimization and evolves into the first single-domain state, known as the flower state. This state is illustrated in Fig. 7 for $N = 9$, $N = 15$, and $N = 21$, all evaluated at $\lambda = 8.00$.

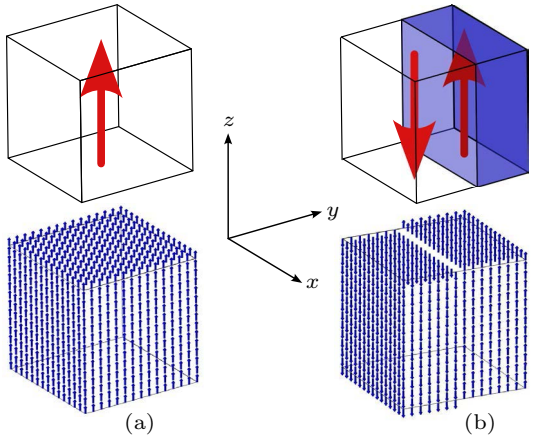


Fig. 6. Initial orientation of the magnetic moments. (a) The magnetic moments are parallel to the easy axis, and (b) half of the moments are antiparallel to the easy axis.

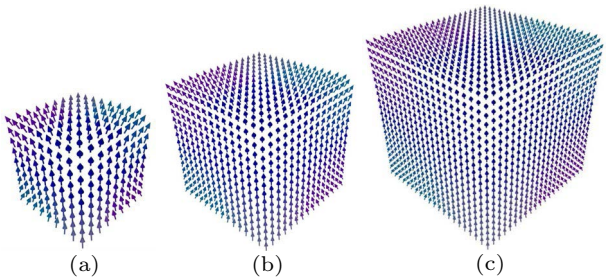


Fig. 7. Uniform domain configuration, referred to as the flower state, observed for (a) $N = 9$, (b) $N = 15$, and (c) $N = 21$, all at fixed length $\lambda = 8.00$.

We observe that the magnetic moments are more inclined at the lateral faces of the cube, while at the center, they are more aligned with the easy axis, as shown in more detail in Fig. 8, highlighting the planes $z = -L/2$, $z = L/2$, and $x = L/2$. Our simulation results are consistent with previously reported studies.[8,9,22–26]

The comparison of the energies of the flower state and the twisted flower state is performed by increasing the value of λ and is shown in the next section. To further analyze the stability of these configurations, we will compare the energies of the flower and twisted flower states as a function of the λ ratio to determine the state change.

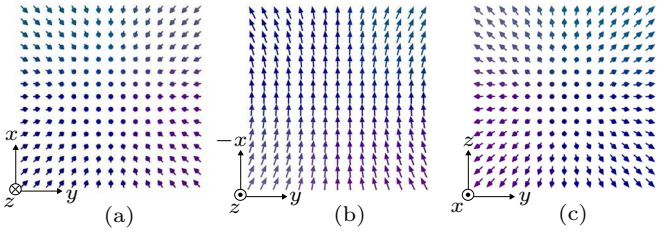


Fig. 8. (a) Bottom view of the cube ($z = -L/2$), showing magnetic moments converging inward. (b) Top view ($z = +L/2$), where the moments emerge outward from the cube surface. (c) Cross-section of the lateral face at $x = +L/2$, illustrating inhomogeneous magnetization near the edges. A similar pattern is observed for $y = \pm L/2$. The configuration corresponds to a system size of $N = 15$ and length parameter $\lambda = 8.00$.

3.2. Twisted flower state

Starting again from the initial configuration shown in Fig. 6(a), and increasing the values of ξ to determine higher values of λ, the system begins to exhibit instability. The total magnetization rearranges to minimize the total energy, resulting in the twisted flower state, as shown in Fig. 9 for $N = 9$, $N = 15$, $N = 21$. All configurations correspond to $\lambda = 8.20$.

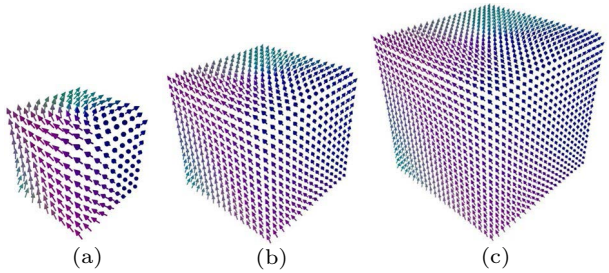


Fig. 9. Twisted flower state displayed as a uniform magnetization configuration for system sizes (a) $N = 9$, (b) $N = 15$, and (c) $N = 21$, with all cases computed at $\lambda = 8.20$.

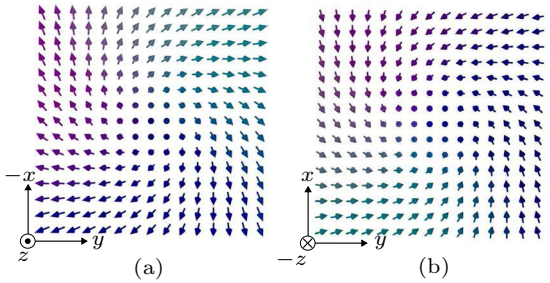


Fig. 10. (a) Top-face projection ($z = +L/2$) and (b) bottom-face projection ($z = -L/2$) of the cube in the twisted flower state, for a system size of $N = 15$ and length parameter $\lambda = 8.20$.

The two states are similar, with the difference that the twisted flower state exhibits a greater deformation of the magnetization relative to the easy axis. This can be observed in Figs. 10 and 11, which show cross-sectional views of the faces

along the z and x directions for the twisted flower state. This behavior is also evident for the system sizes $N = 9$ and $N = 21$, as previously described in Fig. 9.

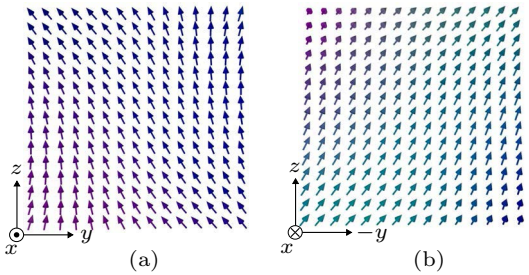


Fig. 11. Side view of the cube in the twisted flower state at (a) $x = +L/2$ and (b) $x = -L/2$, for a system size of $N = 15$. These cross-sectional profiles, obtained at $\lambda = 8.20$, are also representative of the magnetization behavior on the lateral faces at $y = \pm L/2$.

Figure 10 shows the magnetization forming a spiral or vortex at the top surface of the cube, while on the side faces of Fig. 11 the magnetic vector is inclined relative to the z-axis. When observing the cross-section at $x = 0$ in Fig. 12, we obtain a perspective identical to the image of the side face of the cube in the flower state (Fig. 8).

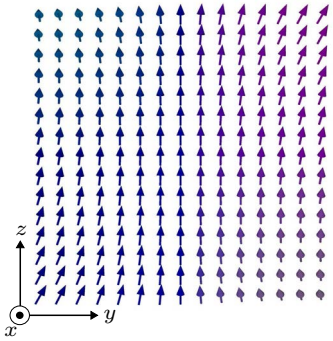


Fig. 12. Mid-plane $x = 0$ cross-section of the twisted flower state, obtained for $N = 15$ at $\lambda = 8.20$.

The change of state can be verified by measuring either the magnetization m_z or the energy as a function of λ. Figure 13 shows the magnetization m_z as a function of λ (for $N = 9$, 15 and 21), allowing verification of the transition between the two states.

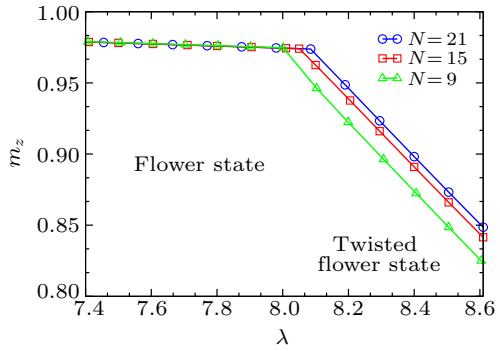


Fig. 13. Out-of-plane magnetization component m_z as a function of λ for grids with $N = 9$, $N = 15$, and $N = 21$, highlighting the transition from the flower state to the twisted flower state. This transition occurs at approximately $\lambda = 8.00$, $\lambda = 8.05$, and $\lambda = 8.08$, respectively.

This transition is further supported by energy analyses, with Fig. 14 presenting results for $\lambda = 8.08$ and Fig. 15 for $\lambda = 8.20$, both simulated with $N = 21$ using the initial configuration shown in Fig. 6(a). For $\lambda = 8.08$, the energy reaches its minimum at the beginning of the simulation and remains stable throughout, confirming a transition to the stable ground state. In contrast, at $\lambda = 8.20$, the system initially relaxes into a metastable flower state, characterized by a well-defined energy plateau, as can be seen in Fig. 15. Subsequently, a pronounced drop in energy marks the transition to the lower-energy twisted flower state.

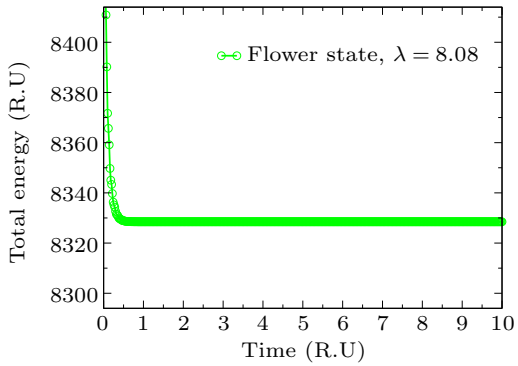


Fig. 14. Total energy minimization over time in the flower state at $\lambda = 8.08$ for grid size $N = 21$.

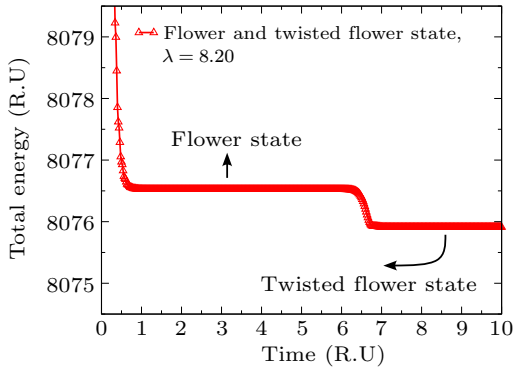


Fig. 15. Total energy minimization over time for the cube with grid size $N = 21$ in the flower and twisted flower states at $\lambda = 8.20$, resulting in a single energy curve.

From this analysis, we conclude that the twisted flower state is more energetically favorable than the flower state. This state was first reported by Schabes *et al.*,[1] who initially referred to it as the vortex state due to the observed image along the z-axis and later renamed it the twisted flower state. Hertel *et al.*[9] found the twisted flower state for $\lambda \approx 8.60$. Vansteenkiste *et al.*,[22] Makarov[26] and Guanghui *et al.*[23] found, respectively, $\lambda = 8.16$, $\lambda = 8.25$ and $\lambda = 8.40$. Based on our simulations for $N = 9$, $N = 15$, and $N = 21$, we found that the flower state remains stable up to $\lambda = 8.00$, $\lambda = 8.05$, and 8.08, respectively. For slightly higher values of λ, the configuration is changed to the twisted flower state. These transition thresholds are in good agreement with those reported by the aforementioned authors.

4. Vortex state

In simulations using the LLG equation, the absence of transitions from the flower state to the vortex state or from the twisted flower state to the vortex state is due to a gap energy that cannot be overcome using micromagnetism. For this reason, we used the initial configuration shown in Fig. 6(b)[9] to achieve the vortex state with the lowest energy. This allowed us to compare the energies of the three states — flower, twisted flower, and vortex — and determine which one has the lowest energy. In this final equilibrium state, the magnetic moment vector circulates around the x-axis, as shown in Fig. 16 for three planes perpendicular to the x-axis ($x = L/2$, $x = 0$, and $x = -L/2$). Figure 17 shows three planes perpendicular to the y-axis ($y = L/2$, $y = 0$, and $y = -L/2$), where it is evident that there is a component of the magnetic moment along the x-axis in Fig. 17(b).

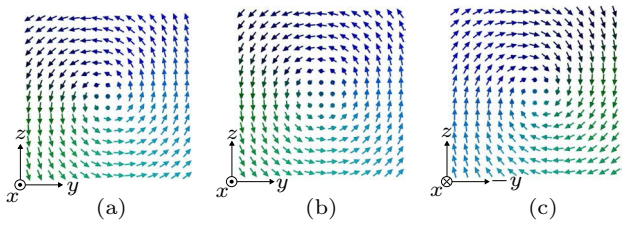


Fig. 16. Cross-sectional views of the cube for the vortex state for a system with $N = 15$ and $\lambda = 8.20$: (a) side face at $x = +L/2$, (b) mid-plane at $x = 0$, and (c) side face at $x = -L/2$.

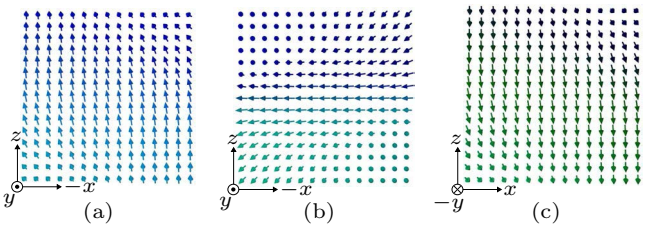


Fig. 17. Representative cross-sections of the cube for the vortex state along the y-direction for a system with $N = 15$ and $\lambda = 8.20$: (a) face at $y = +L/2$, (b) mid-plane at $y = 0$, and (c) face at $y = -L/2$.

This alignment (magnetization perpendicular to the easy axis) is known in the literature as the Bloch line.[27] Similar results were reported by Hertel *et al.*[9] and Schabes *et al.*[1] Figure 18 shows our results of simulations for $N = 21$, conducted to determine which state has the lowest energy. The figure shows the energy values for the flower, twisted flower, and vortex states at three different values of λ: 8.40, 8.41, and 8.44. For $\lambda = 8.40$ (Fig. 18(a)), the twisted flower state exhibits the lowest energy, whereas the vortex state has the highest energy. At $\lambda = 8.41$ (Fig. 18(b)), the twisted flower state remains the lowest energy configuration, but the flower state now becomes the highest in energy. Finally, for $\lambda = 8.44$ (Fig. 18(c)), the vortex state changes to the lowest-energy state, while the flower state becomes the highest. This analysis of the system energy allows us to accurately verify the transition between states of equilibrium configurations.

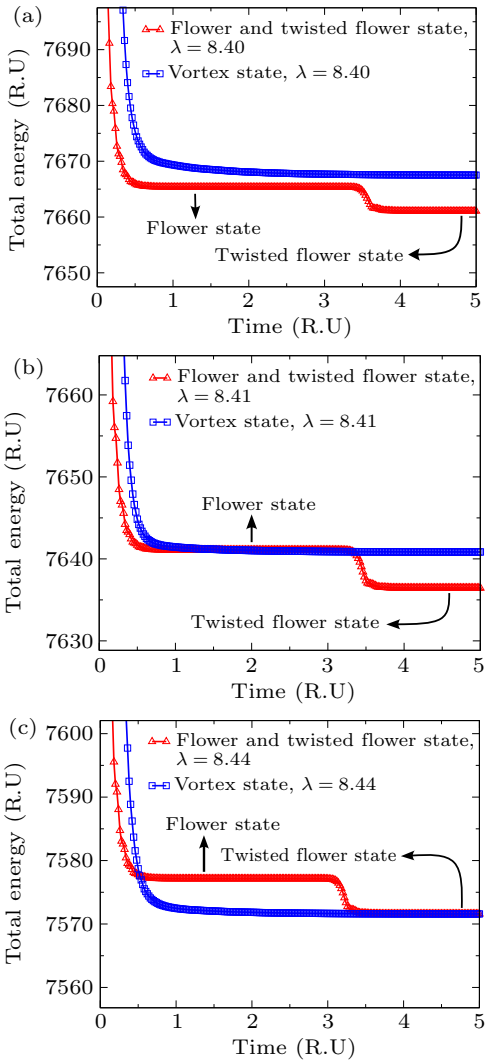


Fig. 18. Total energy as a function of time for grid $N = 21$, comparing the flower, twisted flower, and vortex states at different lengths: (a) at $\lambda = 8.40$, the vortex state remains energetically higher, while the twisted flower state emerges after the initial plateau; (b) at $\lambda = 8.41$, the twisted flower state exhibits the lowest energy, with the flower state being more energetic than the vortex; (c) at $\lambda = 8.44$, the twisted flower state becomes less favorable than the vortex, which then becomes the energetically preferred configuration.

Our results further demonstrate that λ is system-size dependent. And as shown in Fig. 19, λ exhibits a clear asymptotic convergence with increasing N, approaching a limiting value of $\lambda \approx 8.45$. Given that for $N > 17$, λ varies only in the second decimal place, this indicates stabilization.

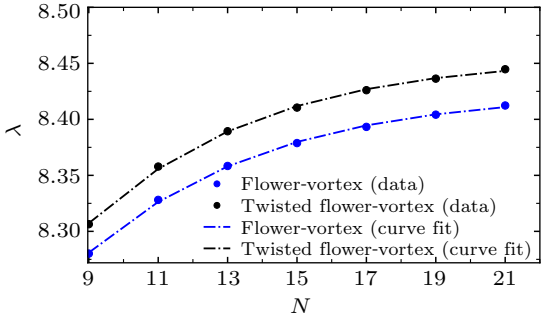


Fig. 19. Variation of the characteristic length λ with the number of simulation cells N, highlighting the energetic transition between the flower-vortex state and the twisted flower-vortex state. The dash-dotted lines in the figure are guide for the eyes.

Table 1 summarizes the values of λ reported in the literature for the twisted flower-to-vortex transition, as well as our result. As can be seen, our results are in excellent agreement with the established data.

Table 1. Comparison between results obtained in this work and results found in the literature.

Authors	λ
Rave; Fabian; Hubert[8]	8.47
Hertel; Kronmuller[9]	8.56
Vansteenkiste *et al.*[22]	8.47
Guanghui Hu *et al.*[23]	8.48
Bjørk *et al.*[24]	8.47
Ribeiro; Freitas; Martins[25]	8.46
Makarov[26]	8.43
GFMC-UFJF	8.45

5. Conclusion

We performed micromagnetic simulations of cubic particles to investigate minimum-energy states following standard problem No. 3 where the magnetostatic energy of the system was calculated using the conventional approach for magnetic moments distributed across a discrete lattice. Our results successfully identified the three fundamental low-energy states — flower, twisted flower, and vortex states — in agreement with established literature.[8,9,22–26] For the largest system analyzed ($N = 21$ cells), the transition between the twisted flower and vortex states occurred at $\lambda \approx 8.45$, indicating an asymptotic behavior. The obtained configurations for all energy-minimized states are consistent with the published results, as confirmed by the magnetic structures observed in each cube face projection. These results demonstrate that the dipolar-interaction based approach achieves high accuracy and excellent agreement with the results found in the literature. This confirms its suitability for realistic micromagnetic simulations and validates the reliability of our computational implementation.

Program availability

The relevant program GFMC-UFJF is openly available on GitHub at https://github.com/pzcoura/micromagnetism-simulation-GFMC-UFJF.git and in the Science Data Bank at https://doi.org/10.57760/sciencedb.j00113.00290.

Acknowledgments

The authors would like to thank CAPES, CNPq, and FAPEMIG (Brazilian Agencies) for their financial support. All numerical simulations were carried out at the Computational Simulation Laboratory of the Department of Physics at UFJF. We are especially grateful to Professor Dr. Fernando Sato for his administrative support of the laboratory.

References

[1] Schabes M E and Bertram H N 1988 *J. Appl. Phys.* **64** 1347
[2] Coey J M D and Parkin S S P 2021 *Handbook of Magnetism and Magnetic Materials* 1st edn (Switzerland: Springer)
[3] Brown Jr W F 1978 *J. Appl. Phys.* **49** 1937
[4] Bagnéres-Viallix A, Baras P and Albertini J B 1991 *IEEE Trans. Magn.* **27** 3819
[5] Krüger B, Selke G, Drews A and Pfannkuche D 2013 *IEEE Trans. Magn.* **49** 4749
[6] Exl L and Schrefl T 2014 *J. Comput. Phys.* **270** 490
[7] Wang W, Lyu B, Kong L, Fangohr H and Du H 2024 *Chin. Phys. B* **33** 107508
[8] Rave W, Fabian K and Hubert A 1998 *J. Magn. Magn. Mater.* **190** 332
[9] Hertel R and Kronmüller H 2002 *J. Magn. Magn. Mater.* **238** 185
[10] McMichael R D µMag Standard Problems (1998) Accessed: January 28, 2024
[11] Brown Jr W F *Micromagnetics* (New York: Wiley) 1963
[12] Brown Jr W F and La Bonte A E 1965 *J. Appl. Phys.* **36** 1380
[13] Ivanov Y P and Chubykalo-Fesenko O 2015 *Magnetic Nano- and Microwires* (Cambridge: Woodhead Publishing) pp. 423–448
[14] Toscano D, Leonel S A, Dias R A, Coura P Z, Rocha J C S and Costa B V 2011 *J. Appl. Phys.* **109** 014301
[15] Toscano D, Leonel S A, Dias R A, Coura P Z and Costa B V 2011 *J. Appl. Phys.* **109** 076104
[16] Farias W S, Santece I A and Coura P Z 2023 *J. Magn. Magn. Mater.* **568** 170386
[17] Gilbert T L 2004 *IEEE Trans. Magn.* **40** 3443
[18] Santece, I A and Gomes, J C S and Toscano, D and Monteiro Jr, M G and Mendonça, J P A and Araujo, C I L and Sato, F and Leonel, S A and Coura, P Z 2020 *QUARKS Brazilian Electronic Journal of Physics Chemistry and Materials Science.* **2674–9688**
[19] Torres, L and Lopez-Diaz, L and Martinez, E and Alejos, O 2012 *IEEE Transactions on Magnetics* **39** 5
[20] Giordano, A and Finocchio, G and Torres, L and Carpentieri, M and Azzerboni, B 2012 *J. Appl. Phys.* **111** 07D112
[21] Raimondo E, Darwin E, Rodrigues D, Giordano A, Carpentieri M, Finocchio G, Tomasello R 2024 *IEEE 24th International Conference on Nanotechnology (NANO)* 191–195
[22] Vansteenkiste A, Leliaert J, Dvornik M, Garcia-Sanchez F and Van Waeyenberge B 2014 *AIP Adv.* **4** 107133
[23] Yang L, Chen J and Hu G 2021 *J. Comput. Phys.* **431** 110142
[24] Bjørk R, Poulsen E B, Nielsen K K and Insinga A R 2021 *J. Magn. Magn. Mater.* **535** 168057
[25] Ribeiro F, Freitas P P and Martins J L 1999 *J. Appl. Phys.* **85** 5810
[26] Makarov A 2014 *Modeling of Emerging Resistive Switching Based Memory Cells* (Vienna: E360 - Institut für Mikroelektronik)
[27] Izmozherov I M, Zverev V V and Baykenov E Z 2019 *J. Phys.: Conf. Ser.* **1389** 012002